

DETERMINATION OF A SHAPE AND SIZE INDEPENDENT MATERIAL MODULUS FOR HONEYCOMB STRUCTURES IN ADDITIVE MANUFACTURING

Thao Le^{*}, Dhruv Bhate[†], John M. Parsey, Jr.^{*}, Keng H. Hsu^{*}

^{*}Arizona State University, Mesa, AZ

[†]Phoenix Analysis & Design Technologies Inc. (PADT), Tempe, AZ

Abstract

Most prior work on modeling cellular structures either assumes a continuum model or homogenizes “effective” cell behavior. The challenge with the former is that bulk properties do not always represent behavior at the scale of the cellular member, while homogenization results in models that are shape specific and offer little insight into practical design matters like transitions between shapes, partial cells or skin junction effects. This paper demonstrates the strong dependence of measured properties on the size of the honeycomb specimen used for experimental purposes and develops a methodology to extract a material modulus in the presence of this dependence for three different honeycomb shapes. The results in this paper show that the extracted modulus for each shape converges as the number of cells in the specimen increases and further, that the converging values of the material moduli derived from the three shapes are within 10% of each other.

Introduction: The Role of Modeling

It is well appreciated that cellular structures such as honeycombs and lattices are a particularly exciting research frontier in Additive Manufacturing (AM). Broadly speaking the research landscape in this space involves design, manufacturing, modeling and implementation into an application. Several software solutions enable design with cellular structures and the published literature on manufacturing them is rapidly growing. This work focuses on the modeling aspects of cellular structures produced with AM. Modeling in this context is the analytical representation of material behavior, primarily for use in predictive analysis. This is a critical aspect of enabling true simulation-driven design, where the design is the outcome of some objective such as stiffness-to-weight maximization relative to an allowable stress. From a more abstract point of view, modeling links up design and manufacturing capabilities to the application. Without models that describe cellular structure behavior, we have design tools that make structures that we can even manufacture, but we have little confidence in their ability to perform the desired function in the end-application, especially when these are critical to function. While it is possible to certify components with cellular structures through rigorous testing, valid models and robust simulation together can both drive down qualification costs and unlock untapped potential that a normal design-manufacture-test cycle fails to uncover.

Approaches to develop predictive models for cellular materials fall into three broad categories depending on the level of discretization at which the property is modeled: at the level of the individual unit cell, at the level of the connecting member or finally, at the level of each material

point. The most straightforward approach is to use bulk material properties to represent what is happening to the material at the cellular level [1-4]. This approach does away with the need for any cellular level characterization and in so doing, does not have to account for size or contact effects described previously that are artifacts of having to characterize behavior at the cellular level. However, the assumption that the connecting members in a cellular structure behave the same way the bulk material does can be particularly erroneous for AM processes that often introduce significant size specific behavior and large anisotropy. It is important to keep in mind that factors that may not be significant at a bulk level (such as surface roughness, local microstructure or dimensional tolerances) can be very significant when the connecting member is several millimeters thick or less, as is often the case. The level of error introduced by a continuum assumption is likely to vary by process: polymeric processes like Fused Deposition Modeling (FDM) are strongly anisotropic with highly geometry-specific meso-structures and an assumption like this will generate large errors. On the other hand, it is possible that better results may be had for powder based fusion processes used for metal alloys, especially when the connecting members are large enough and the key property being solved for is mechanical stiffness (as opposed to fracture toughness or fatigue life).

A common approach in the literature that attempts to account for behavior at these smaller scales is the use of homogenization, which involves representing the effective property of the cellular structure without explicitly accounting for the cellular geometry itself. This approach has significantly lower computational expense associated with its implementation in simulation software. Additionally, it is relatively straightforward to develop a model by fitting a power law to experimental data [5-9] as shown in the equation below, relating the effective modulus E^* to the bulk material property E_s and their respective densities (ρ and ρ_s), by solving for the constants C and n .

$$E^* = C E_s \left(\frac{\rho}{\rho_s} \right)^n \quad (1)$$

While a homogenization approach is useful in generating comparative, qualitative data, it has some difficulties as a reliable material model in analysis and simulation. This is primarily because homogenization of cells only works for the specific cell in question - so every new cell type needs to be re-characterized. Additionally, the homogenization of these cells obscures insight into how structures behave in the transition region between different volume fractions or at junctions of cellular members and walls, even if each cell type is calibrated at a range of volume.

The third approach involves describing behavior not at each material point or at the level of the cell, but at a level in-between: the connecting member (also referred to as strut or beam) as shown in Figure 1. This approach has been used by researchers [10-12] and in our previous work as well [13] by invoking beam theory to first describe what is happening at the level of the member and then using that information to build up to the level of the cells. This approach, while promising, has some challenges as well: from a computational standpoint, the validation of these models typically requires a modeling of the full cellular geometry, which can be prohibitively expensive. Additionally, the theory involved in representing member level detail is more complex, makes assumptions of its own (e.g. modeling the "fixed" ends of the beam). It is not clear at the present moment if this is justified by a significant improvement in the model's predictability compared to the above two approaches. This approach does however have the potential to be truly shape

independent since it does not require the assumption of a specific unit cell design and is why it is the method of choice for this work as well.

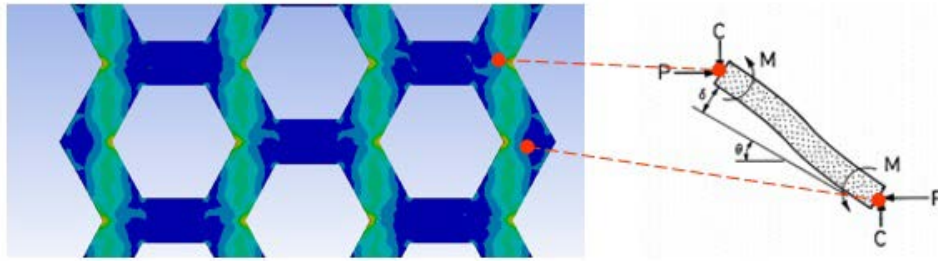


Figure 1. Representation of cellular structures as an assemblage of connecting members such as the beam shown here enables the use of beam theory in the development of models (P and C represent loads, M the moment, θ and δ the angle and displacement of the beam)

Modeling in the Presence of Shape and Size Dependence

There are several challenges associated with modeling cellular structures and materials. Chief among these is the fact that behavior of these structures is highly dependent on the shape of the specific cells used in the structure being studied [13] – in other words, a hexagonal honeycomb structure will behave differently than a square or triangular structure. What is less intuitive is that data obtained from test specimens used to calibrate models is highly dependent on the size of the specimen tested as well. Consider the experimental data shown in Figure 2 for honeycombs tested in compression, showing that the predicted effective modulus increases with increasing number of cells in the axial direction, but reduces (at a lower rate) for increasing number of cells in the transverse direction. Other experimental and numerical (simulation) studies concur with this observation [14-19] and have even shown that the trend and sensitivity of modulus to the number of cells is itself dependent on the shape being studied [20].

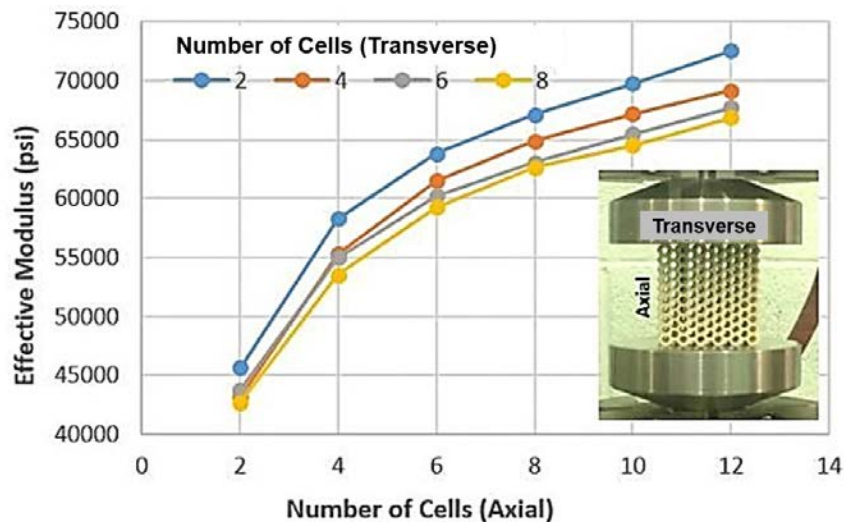


Figure 2. Effective modulus under compression showing a strong dependence on the number of cells in the structure. (The image on the bottom right corner shows a honeycomb sample under a compression test with the Instron 8801 mechanical testing system).

This work focuses on developing a method to establish a shape- and size independent modulus, building on previous work [12] that proposed a method for extracting a material modulus by applying established analytical theory [13] to measure effective behavior of hexagonal honeycomb structures. In this paper, the approach is extended to account for size of specimens (number of cells) and to validate shape insensitivity by comparing results obtained from hexagonal, triangular and square shapes. While the work done here is using the Fused Deposition Modeling (FDM) process, the methodology is expected to be applicable for other manufacturing processes as well.

Specimen Design

The underlying hypothesis of this work is that the material modulus of honeycomb structures with a certain cell geometry will converge to a single value as the number of unit cells approaches “infinity”. Further, this limiting value of the material modulus will be the same for all honeycomb structures regardless of the cell geometry. To test these hypotheses, twenty-five specimens, varying in the number of unit cells, were designed for each geometry group: regular hexagon, square, and equilateral triangle, which are the only three regular two-dimensional space-filling shapes.

Specimens with the regular hexagon geometry had number of cells ranging from 5 to 105, specimens with the square geometry from 16 to 256 cells, and specimens with the equilateral triangle geometry had the number of unit cells ranging from 28 to 460 cells. All of the sample structures were designed using SolidWorks™ with a wall thickness (t) of 0.032", unit length (l) of 0.18", and base width (b) of 1". Three representative CAD models with dimensions for each shape are shown in Figures 3a-c.

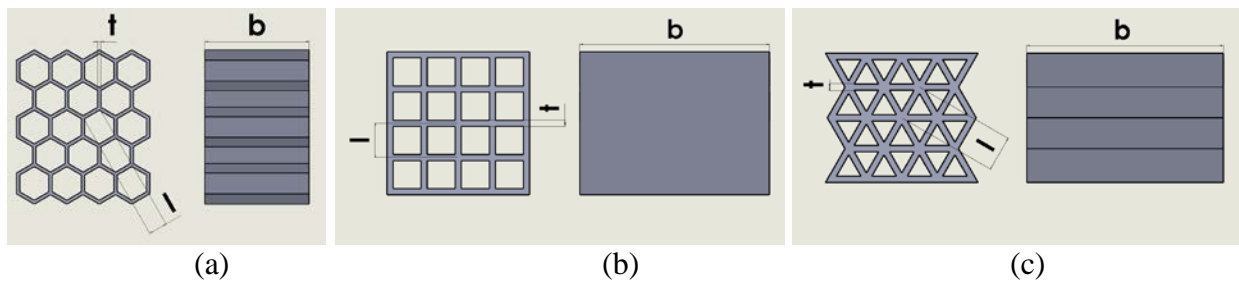


Figure 3. Representative CAD models showing key parameters used in the design for (a) hexagonal, (b) square and (c) triangular honeycomb structures. Note: designs not to scale in above image with respect to each other

Manufacturing and Inspection

The specimens were manufactured using the FDM process on a Stratasys © Fortus™ 400mc machine with ABS-M30™ material. The samples were manufactured in three separate but successive builds on the same machine, using material from a single ABS canister, with the same tip and no re-calibrations performed between builds, to minimize process-induced variation.

The printing parameters used were a layer thickness of 0.010" and a contour width of 0.016", which resulted in 100 layers and a wall thickness of two contours for each specimen. The screenshot of how the filaments were laid out by Stratasys's Insight™ software, and the corresponding printed specimens are shown in Figure 4. A total of 75 specimens were manufactured: 25 per shape. Each of these 75 specimens was unique – in other words, no replications were conducted since the intent of this work was to establish trends in the three shapes as a function of the size of the specimen. These specimens are shown in Figure 5.

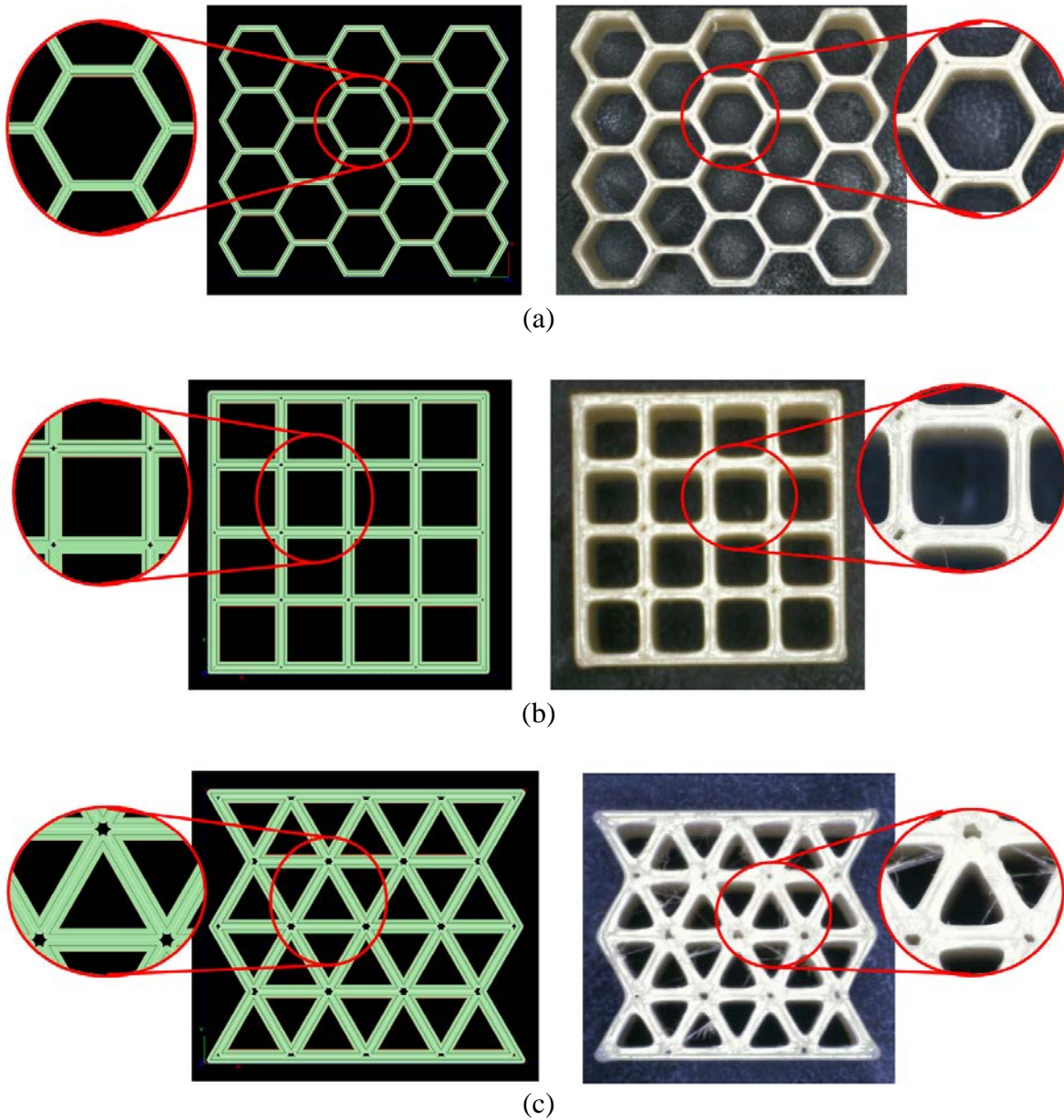


Figure 4. Toolpath (left) and as-printed (right) layers for (a) hexagonal, (b) square and (c) triangular honeycomb structures

A typical industrial FDM process is often capable to dimensional tolerances of approximately 0.005". As a result, for honeycomb structures with small thickness values (0.010-0.070"), this can result in a significantly large percentage of dimensional error. In order to verify the dimensions of these printed structures, four additional specimens from each shape were chosen as representative specimens to be scanned using blue light inspection technique with COMET LED™. Thickness and length measurements were made with Geomagic Control™. The dimensions were measured at multiple locations including both edge and center locations at the top and bottom of the specimens. The findings of this study are summarized in Table 1; details of measurements made and the associated statistical analyses are reported in Appendix A towards the end of this paper. As the results in Table 1 show, the average thickness variation was found to be 0.005" in line with expectations. These values were used in the analytical calculations discussed later in the paper.

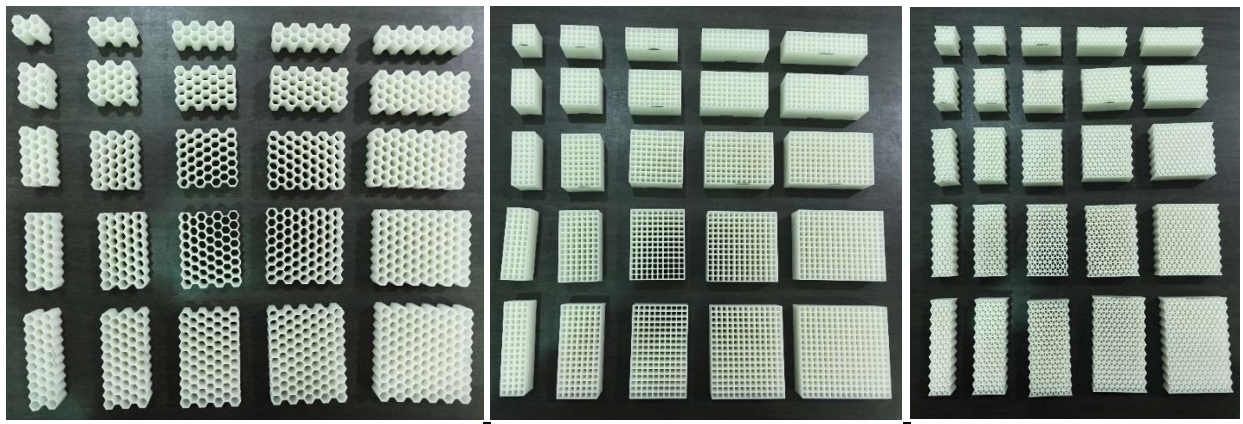


Figure 5. The 75 specimens used in this study – 25 for each of the three shapes: honeycomb (left), square (center), and triangle (right)

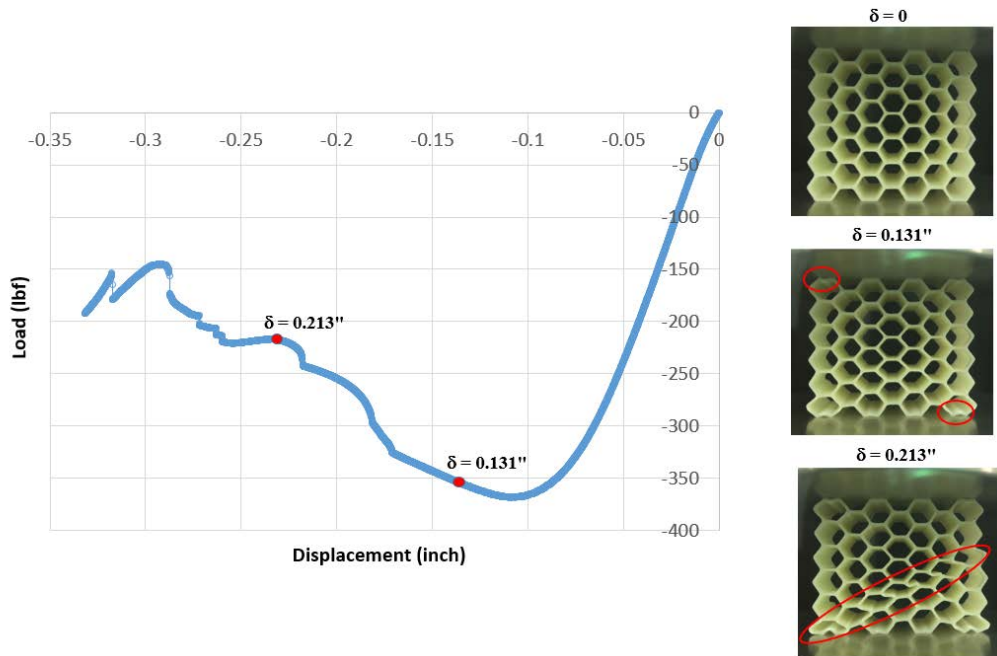
Table 1. Summary of the analysis of the thickness and length of the printed specimens

	Thickness (designed 0.032")		Length (designed 0.18")	
	Mean (in)	Standard deviation (in)	Mean (in)	Standard deviation (in)
Hexagon	0.0315	0.00126	0.1800	0.00018
Square	0.0322	0.00152	0.1802	0.00030
Triangle	0.0316	0.00155	0.1802	0.00020

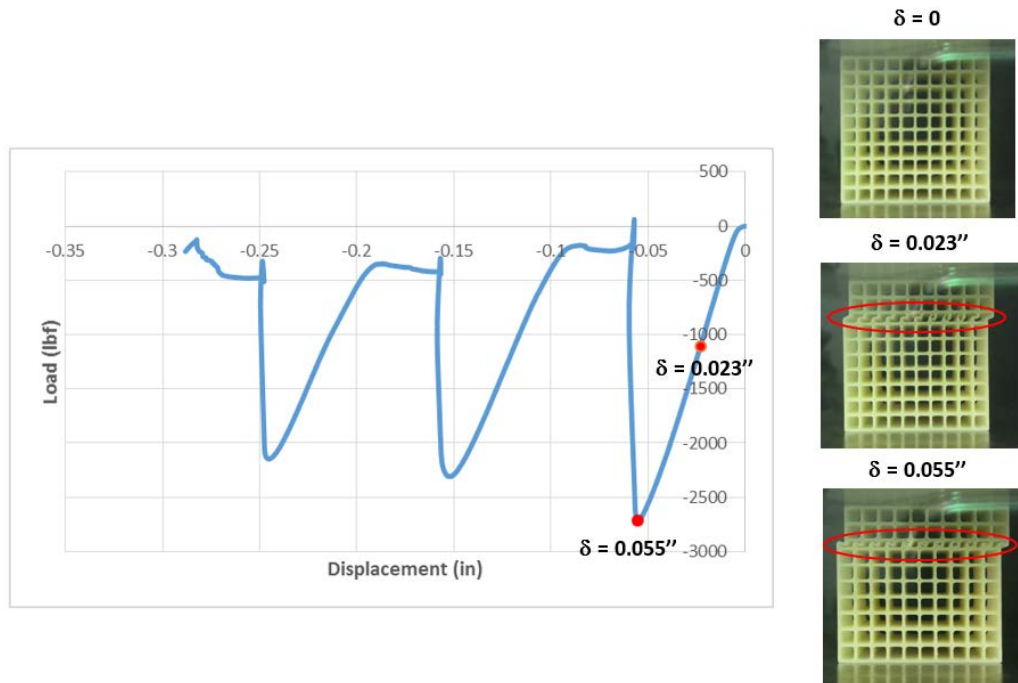
Mechanical Testing

All 75 specimens were tested on an Instron 8801 mechanical testing system operated in compression mode under displacement-control, with a displacement rate of 0.2" per minute, following experimental methods described in previous work [12]. All testing was completed without any changes to the setup of the machine or repositioning of the compression platens.

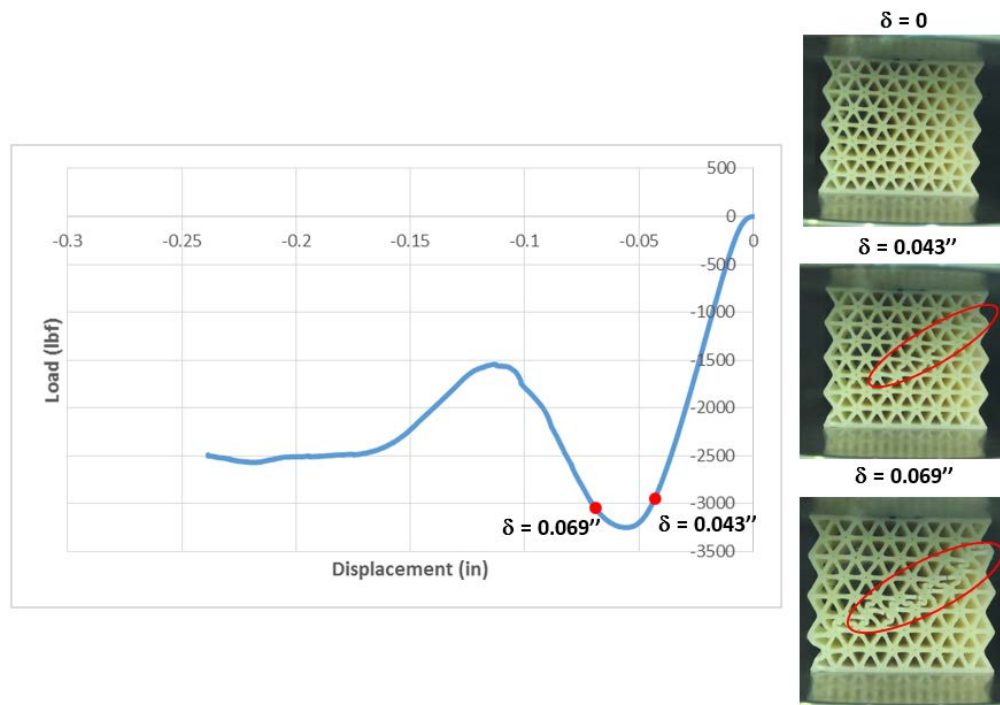
Representative test results from hexagonal, square and triangular honeycomb specimens are shown in Figure 6. The red markers on the graphs correspond to the images captured from a concurrently running video and show how localized deformation in the specimen (encircled in the photographs) relates to observed global deformation. The observed failure mechanism appears consistent with the “plastic hinge” mechanism [13], which is expected for a plastic material such as ABS [21]. Further discussion of the failure mechanism is beyond the scope of the current work, which is concerned with estimation of the modulus only.



(a)



(b)



(c)

Figure 6. Load displacement graph under compression for (a) hexagonal, (b) square and (c) triangular honeycomb specimens. The photographs correspond to the red markers on the graph.

Analysis

The main goal of this approach is to establish a material modulus that is both shape and size independent. To enable this, measured load-displacement responses from these different honeycomb structures need to first be translated into a stress-strain plot and then the modulus calculated. For this purpose, the member modeling method discussed previously and elaborated in previous work [12] was adapted for use here, with two key differences discussed below.

A recent paper by Malek and Gibson [23] corrected the commonly used equations for honeycomb modulus estimation [13] by redefining the length of the connecting members. This corrected length was used in all calculations in this work. For all but the thinnest members, this correction can have a significant effect on modulus calculations (a 10-20% increase). Secondly, this work sought to relate load and displacement at the specimen level to the values at the level of an individual beam. For hexagonal honeycombs loaded in compression, the beam members that are neither parallel nor normal to the applied load (“diagonal” beam members) are the most strained, as shown in Figure 7. This was done to minimize errors associated with defining a specimen area and length for normalization in converting load-displacement to stress-strain. Thus, the total load at the specimen level was divided by the number of beam members that run across the specimen to arrive at a load per beam member. Similarly, the total displacement was divided by the number of diagonal beams to arrive at a displacement per beam member.

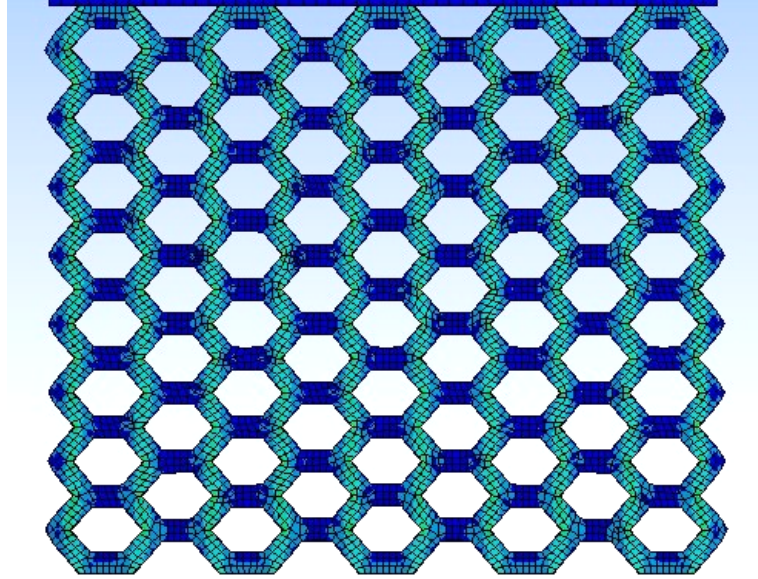


Figure 7. Simulation result of a hexagonal honeycomb specimen under compression showing diagonal beam elements taking up the bulk of the elastic strain

Using this method eliminates the need for defining an effective modulus and only invokes standard beam theory to solve for a material modulus E_s [12, 13]. Thus for a beam member with thickness t , effective length l_b , width b , the material modulus can be described in terms of experimentally measured, beam-level load P and displacement δ , per the equations below:

For hexagonal honeycombs:

$$E_s = \frac{Pl_b^3(\sin 30^\circ)^2}{\delta bt^3} \quad (2)$$

For square honeycombs:

$$E_s = \frac{Pl_b}{\delta bt} \quad (3)$$

For triangular honeycombs:

$$E_s = \frac{Pl_b(\cos 30^\circ)^2}{\delta bt} \quad (4)$$

The effective length l_b follows from Malek and Gibson for hexagonal honeycombs [23] and similar equations can be derived for square and triangular honeycombs. Different approaches were evaluated to quantify the effect of the number of cells on elastic modulus, including using the number of cells in each direction as shown in Figure 1, where the effect of cell quantity on modulus is not the same in both directions. As a result, a new parameter that accounted for both variables together was introduced, which segregates cells in a specimen into partially and fully constrained cells, as shown in Figure 8. This then enables a calculation of a percentage of (fully) constrained cells. The motivation for this approach derives from the fact that analytical equations assume no boundary effects and an infinite number of cells in all directions [13]. Thus, a specimen with 100% percentage of its cells fully constrained would represent the theoretical ideal.

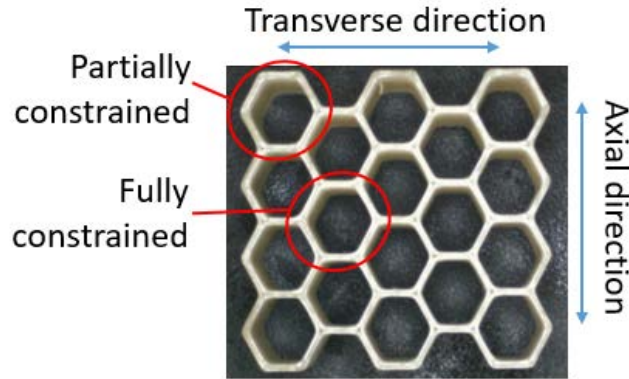


Figure 8. Definition of partially and fully constrained cells and the directions

Using the aforementioned equations, measured load and displacement responses from the compression tests and the dimensions measured using optical scanning, elastic modulus values were computed for each of the 75 samples tested. Each of these data points is plotted in Figure 10 for hexagonal, square and triangular cells. Whereas the general trend is that the estimated material modulus increases as the percentage of constrained cells increases, other interesting trends are also observed and indicated by the alphabetic grouping. These trends, it is hypothesized, emerge as a result of differing edge behaviors in the experiments conducted. As shown in the schematic in Figure 9, cells on the top and bottom are constrained by friction with the compression platens, the cells on the left and right are partially constrained.

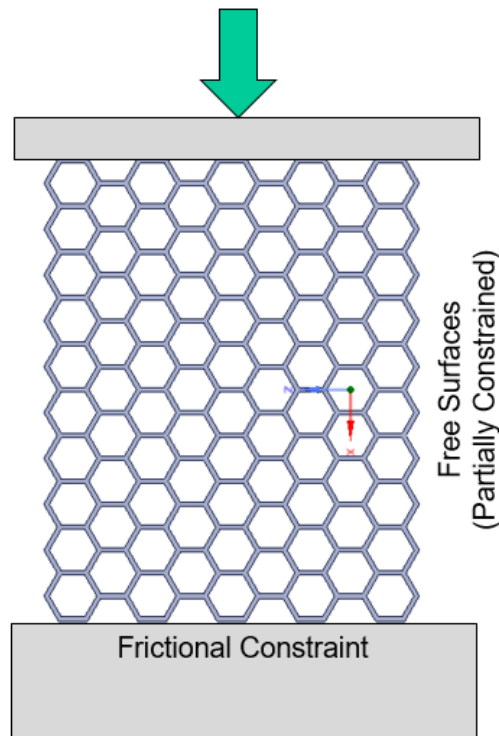
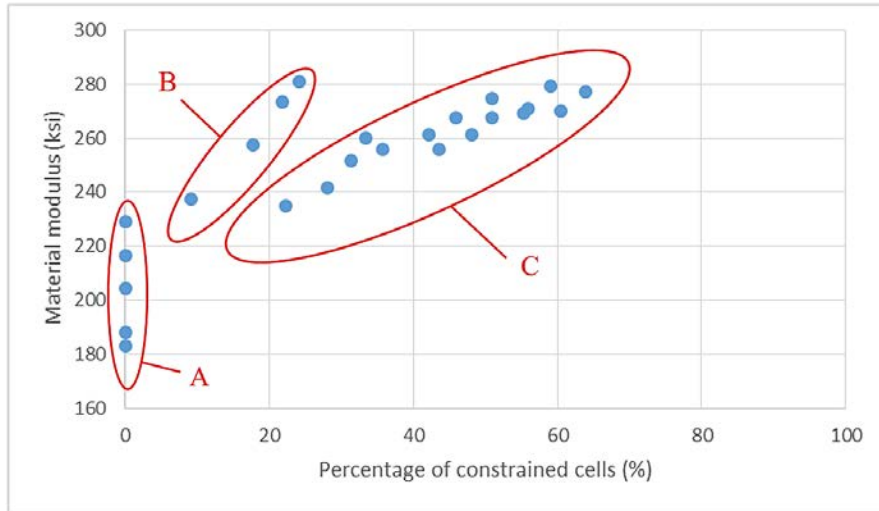
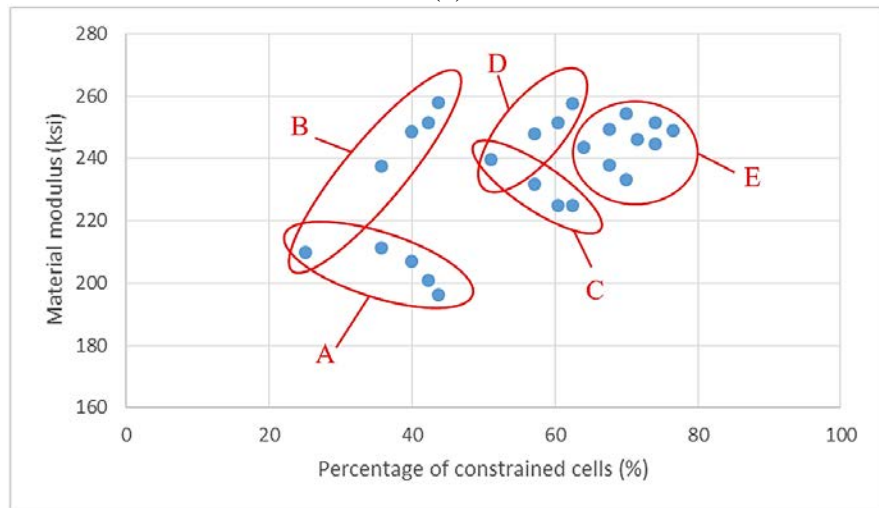


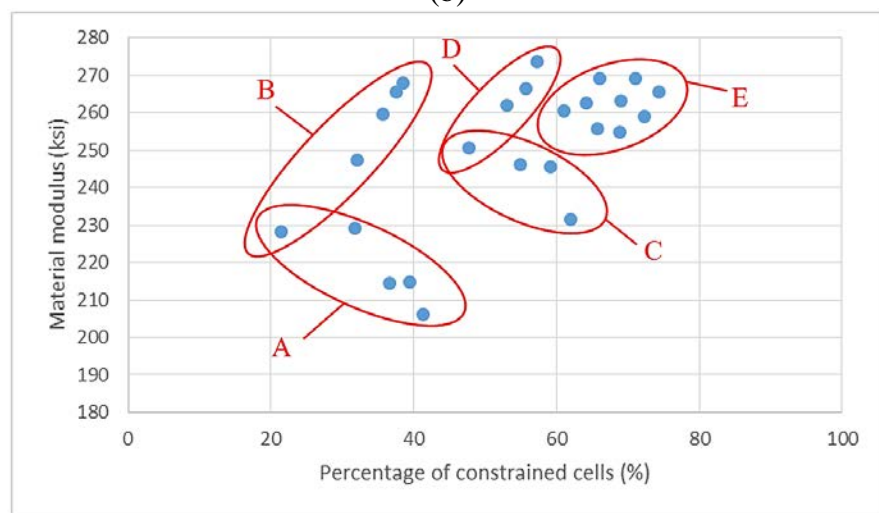
Figure 9. Frictional constraint and free surface (partially constrained cells) create boundary conditions that are not part of the theoretical model and each has a different effect.



(a)



(b)



(c)

Figure 10. Load displacement graph and snapshots in the deformation process under compression for (a) hexagonal, (b) square and (c) triangular honeycomb specimens.

In Figure 10 (a), the specimens in group A had 2 transverse cells, and the specimens in group B had 2 axial cells. Thus the majority of cells in these groups were in contact with the platens (frictional constraint) or had free surfaces (partially constrained). For specimens in group C, the correlation between increasing percentage of constrained cells and modulus is fairly robust. Similar to the hexagonal specimens, the results in Figure 10 (b) showed a divergence in the values of the material modulus for the square specimens that had low percentage of constrained cells. Group A contained all the specimens that had only 4 axial cells, while group B contained all the specimens that had 4 transverse cells. Group C contained all of the specimens that had 7 axial cells, and group D contained all the specimens that had 7 transverse cells. The identical trend was observed for the triangular honeycombs as well in Figure 10 (c). Group A had 4 axial cells, B had 4 transverse cells, C had 8 axial cells and D had 6 transverse cells. The raw data that led to the estimation of these modulus values is compiled in Appendix B.

Results

The trends in Figure 10 are indicative of the core of the challenge this work seeks to address: any measurements of modulus made by characterizing honeycomb structures are strongly dependent on both shape (hexagon, square or triangle) and size (percentage of constrained cells). The hypothesis of this work is that with a member modeling approach that is inherently shape independent, a saturated value of modulus may be extracted for large enough specimens. To determine the validity of this hypothesis with the data in Figure 10, the 95% confidence interval approach was used. The data was compartmentalized in intervals of reducing size (with a decrement of one for each sample, eliminating the point corresponding to the lowest percentage of constrained cells for each iteration) until all the material modulus values extracted from those specimens fell within the range of the 95% confidence interval around their mean. On arriving at this value, it was concluded that the mean of those values could be taken as the representative material modulus. Applying this method to all three shapes resulted in the modulus values in Table 2, which are listed along with the percentage constrained cell values for the specimens that were used to compute the mean modulus.

Table 2. Summary of the analysis of the thickness and length of the printed specimens

	% Constrained Cell Values for Specimen Range in 95% Interval	Extracted material modulus (ksi)	Difference from Hexagonal Honeycomb
Regular hexagon	55-64	273	-
Square	72-77	248	9.2%
Equilateral triangle	68-74	262	4.2%

The agreement of the material modulus extracted from characterization of square and triangular specimens with hexagonal ones is under 10% is a key accomplishment of this work. This difference can be explained by the limited sample size and by the fact that theory assumes cell shapes with sharp corners whereas in reality these have some curvature to them. For a sanity check, bulk ABS values are often reported in the 260-360 ksi range [21], and Stratasys© reports values of 310-320 ksi for specimens made with the FDM process [23] – both these numbers are

close to the values reported in Table 2. In addition to the causes for difference described above, the beam geometries are also not perfectly rectangular as theory assumes, which could be an additional reason why values are different from bulk values.

Conclusions

The following conclusions may be drawn from this work:

1. This work confirms experimentally previously documented observations that modulus estimations for cellular structures are highly dependent on the size of the sample used for characterization.
2. This work also shows how using a beam-modeling approach, with the correct definition of beam length and calculating beam-level load and displacement from experimental measurements, can be used to extract a material modulus that is shape independent.
3. Using a metric of percentage of constrained cells and measuring modulus enables the monitoring of these trends and further find near-saturation values that approach size independence.

Extracted values of modulus using this approach from different shapes and sizes are within 10% of each other – and may be used with greater confidence for non-uniform geometries such as Voronoi cells, as long as they have the same inherent beam-level structure that was characterized to extract the modulus. This approach can be extended to cellular structures of different materials and AM processes, and it is likely to be successful for failure prediction as well.

Acknowledgement

This effort was performed through the National Center for Defense Manufacturing and Machining under the America Makes Program entitled “A Non-Empirical Predictive Model for Additively Manufactured Lattice Structures” and is based on research sponsored by the Air Force Research Laboratory under agreement number FA8650-12-2-7230. The U.S. Government is authorized to reproduce and distribute reprints for Governmental purposes notwithstanding any copyright notation thereon.

Disclaimer

The views and conclusions contained in this document are those of the authors and should not be interpreted as necessarily representing the official policies, either expressed or implied, of the Government. Distribution authorized to U.S. Government Agencies and America Makes Members; Critical Technology. Other requests for this document shall be referred to AFRL/RXMS, Wright-Patterson Air Force Base, OH 45433-7750.

Appendix A: Dimensional Data

This appendix provides data on the measurements made using blue light scanning to extract true, as-printed dimensions. These dimensions (and not as-designed values) were used in the analysis.

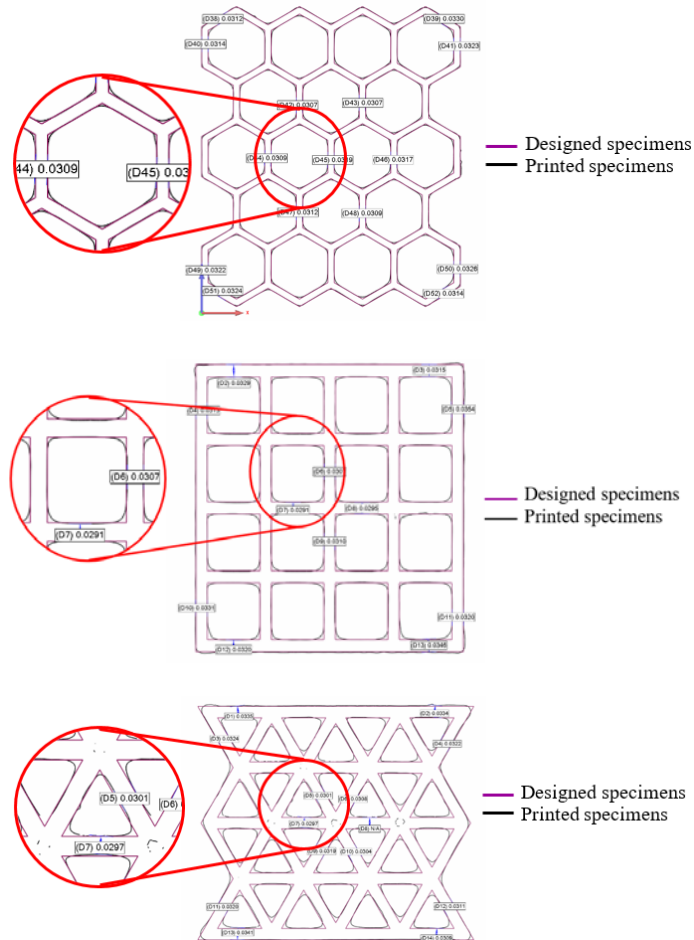


Figure A1. Designed and scanned data superimposed, measurements made with Geomagic Control™

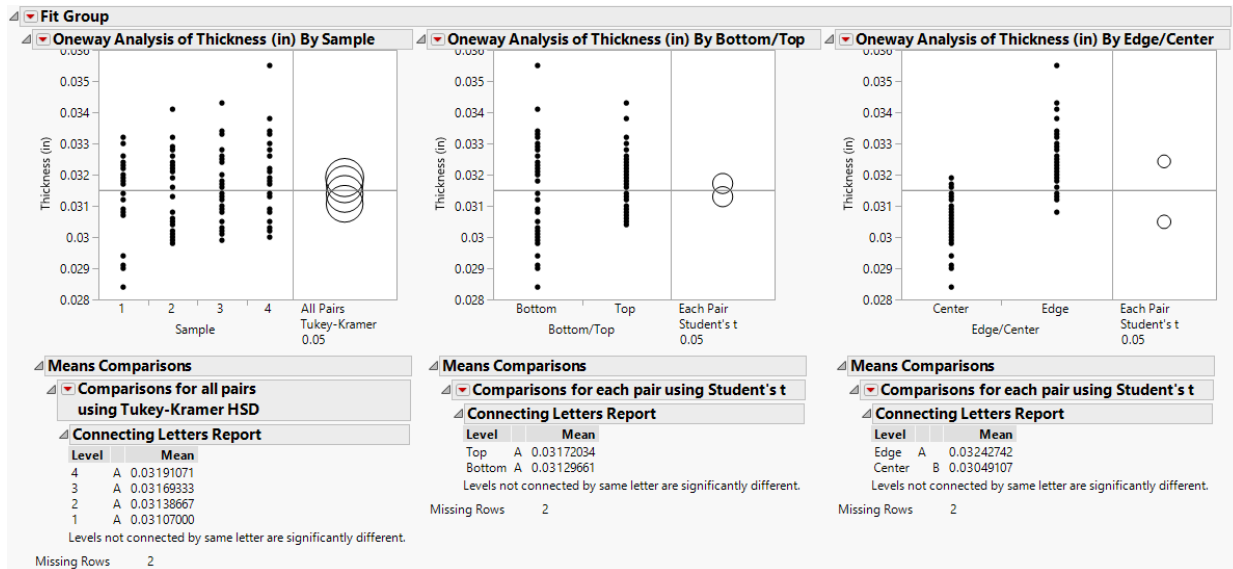


Figure A2. Analysis of the thickness of the regular hexagon specimens. Of note is the difference in the means comparisons for bottom/top and center/edge.

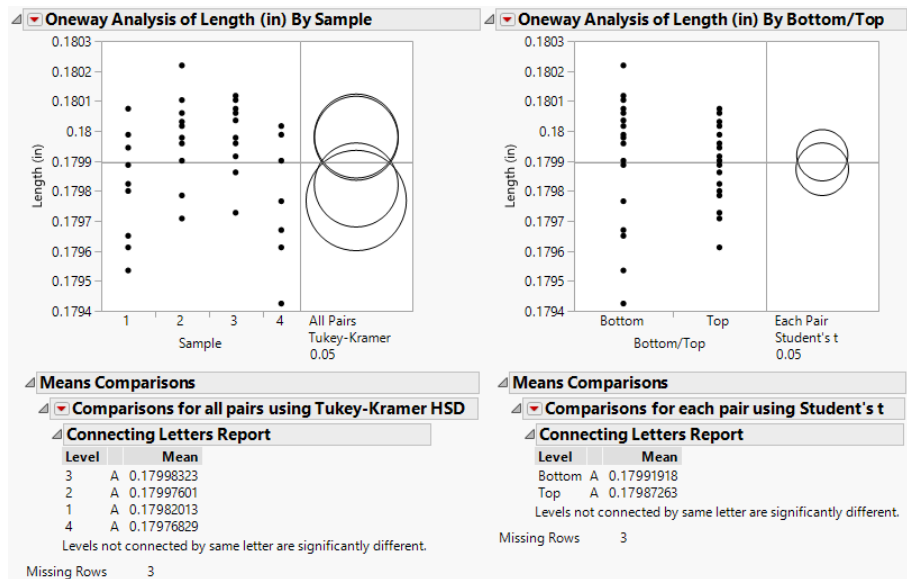


Figure A3. Analysis of the length of the regular hexagon specimens

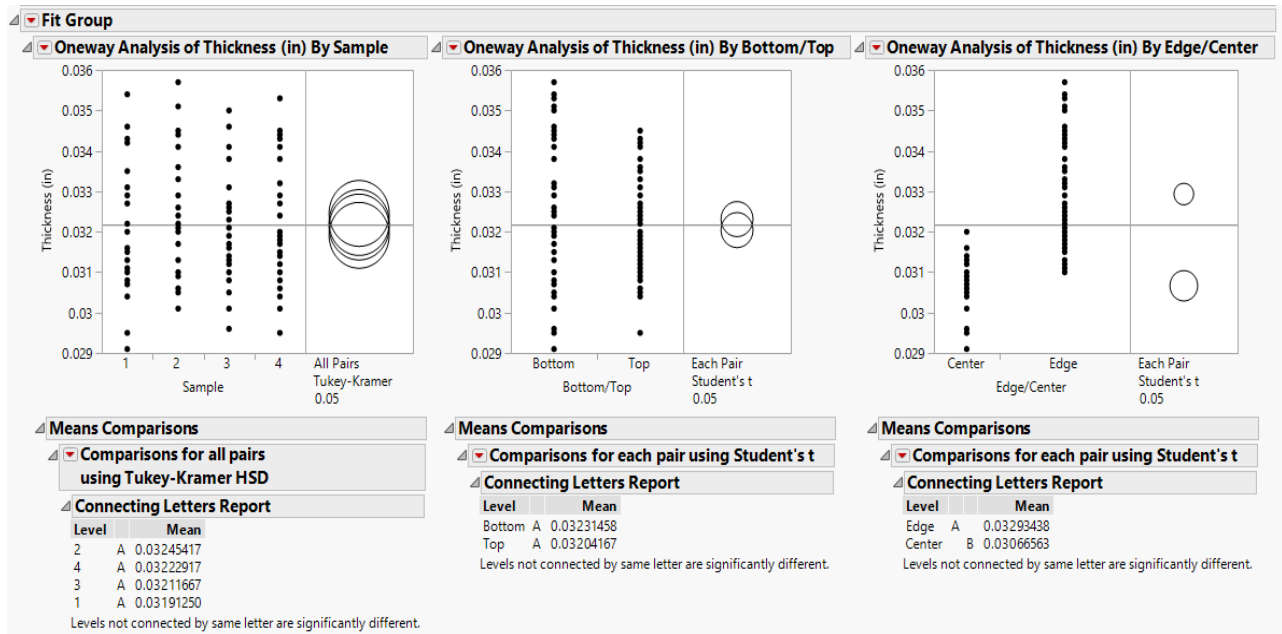


Figure A4. Analysis of the thickness of the square specimens. Of note is the difference in the means comparisons for bottom/top and center/edge.

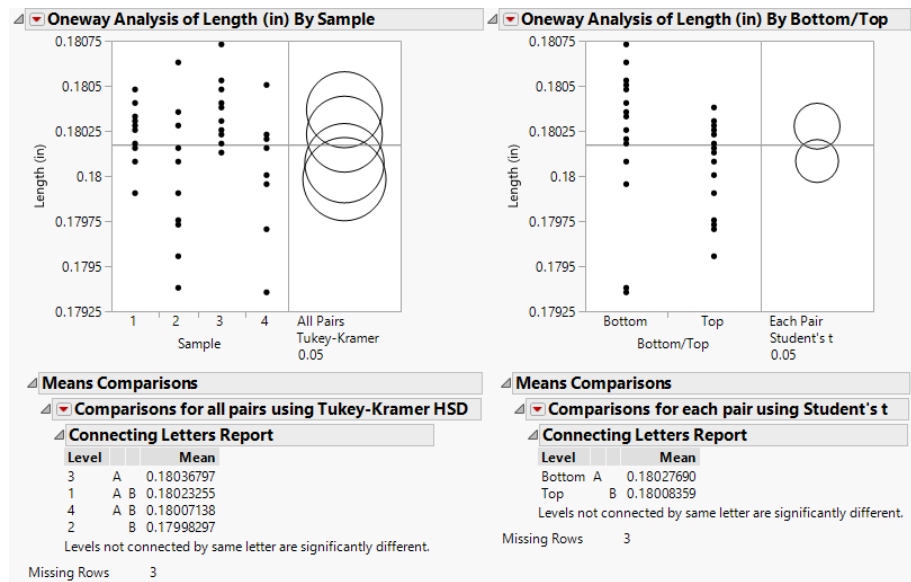


Figure A5. Analysis of the length of the square specimens

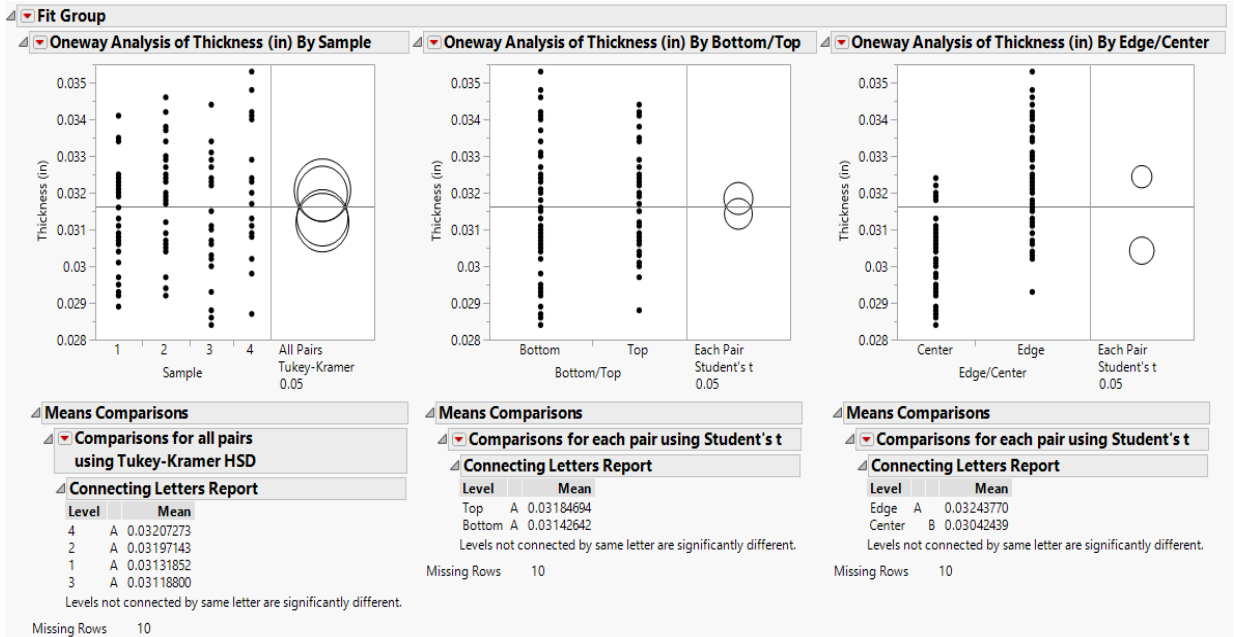


Figure A6. Analysis of the thickness of the equilateral triangle specimens. Of note is the difference in the means comparisons for bottom/top and center/edge.

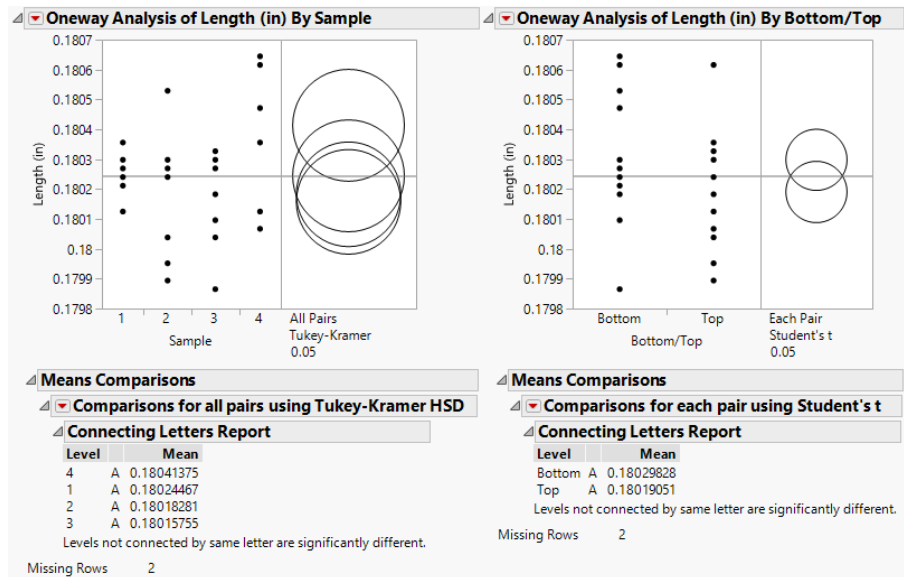


Figure A7. Analysis of the length of the equilateral triangle specimens.

Appendix B: Compression Test Data

This appendix provides the load-displacement data for all 75 samples tested – to make viewing easier, each shape is broken down into 3 categories corresponding to the percentage of constrained cells in those specimen designs.

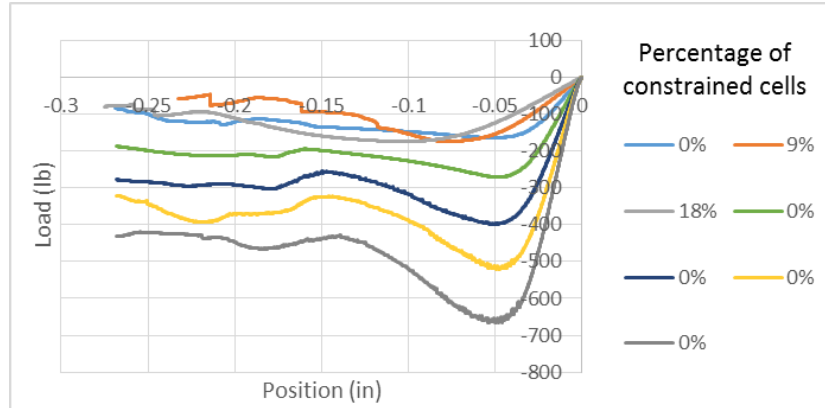


Figure B1. Graphs of load vs. position of regular hexagon specimens that had 0-20% of constrained cells.

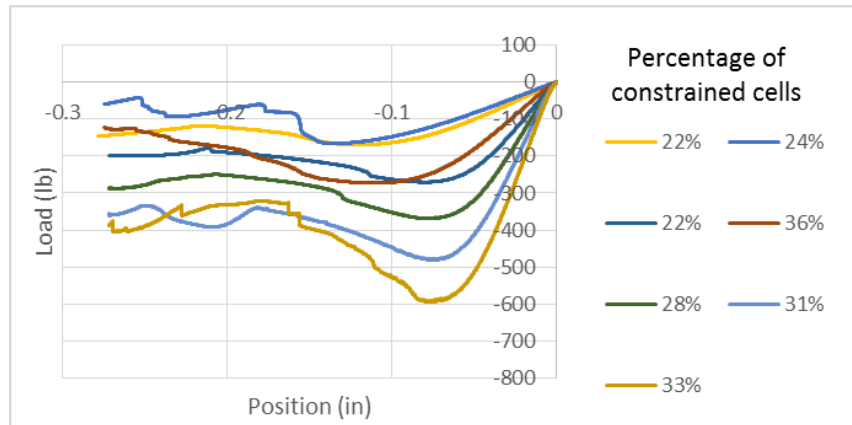


Figure B2. Graphs of load vs. position of regular hexagon specimens that had 21-40% of constrained cells.

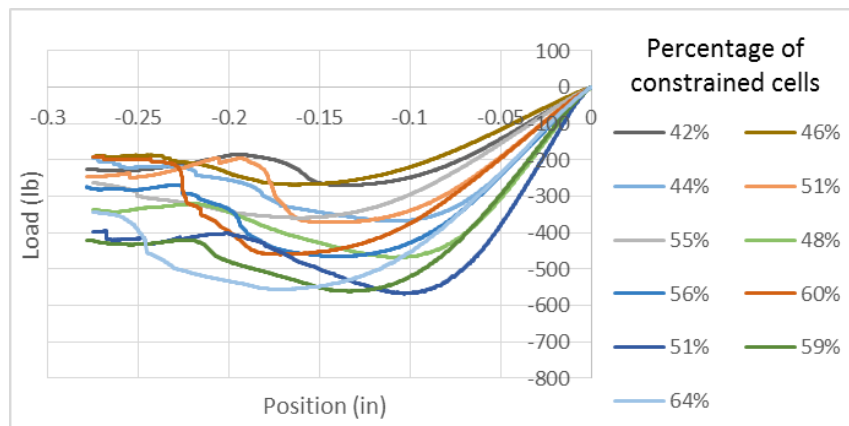


Figure B3. Graphs of load vs. position of regular hexagon specimens that had more than 40% of constrained cells.

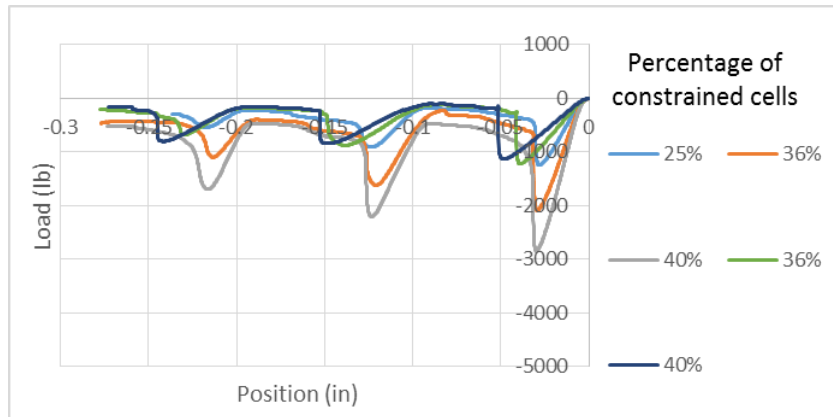


Figure B4. Graphs of load vs. position of square specimens that had 20-40% of constrained cells.

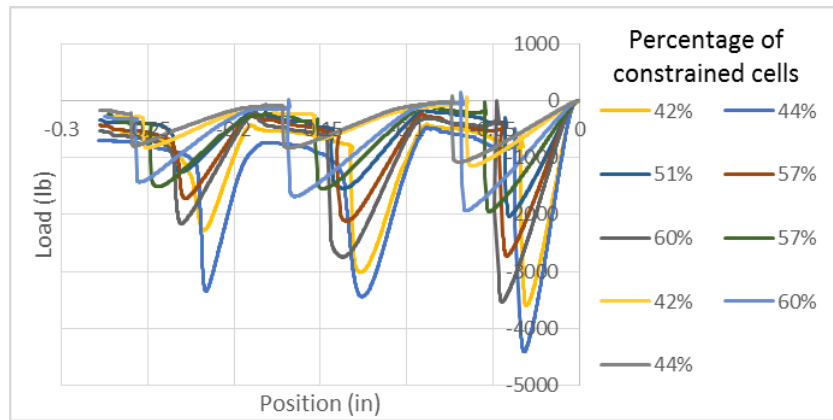


Figure B5. Graphs of load vs. position of square specimens that had 41-60% of constrained cells.

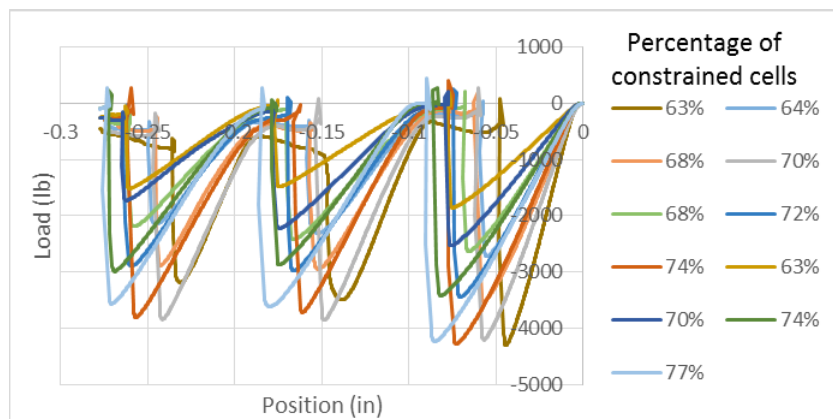


Figure B6. Graphs of load vs. position of square specimens that had more than 60% of constrained cells.

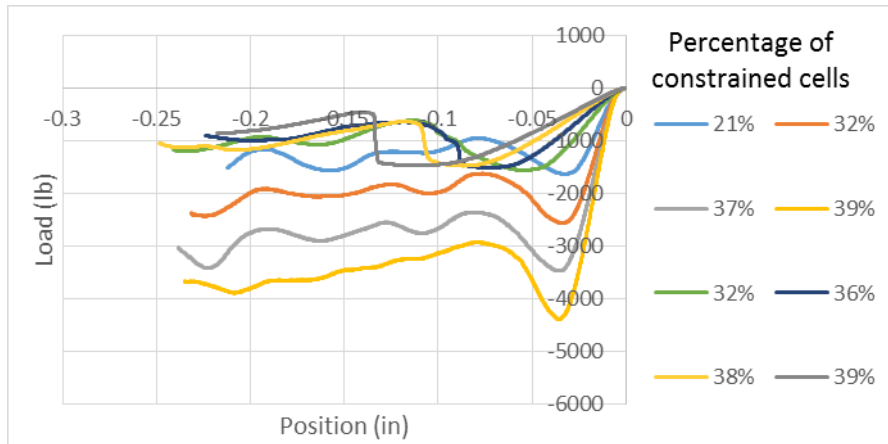


Figure B7. Graphs of load vs. position of equilateral triangle specimens that had 20-40% of constrained cells.

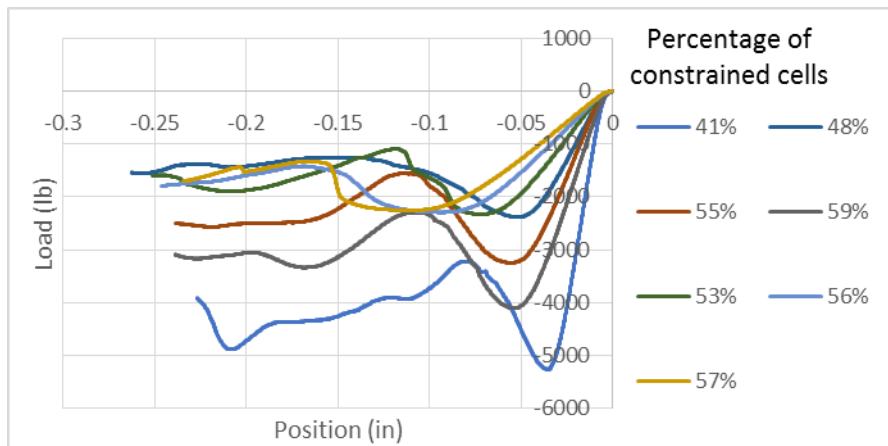


Figure B8. Graphs of load vs. position of equilateral triangle specimens that had 41-60% of constrained cells.

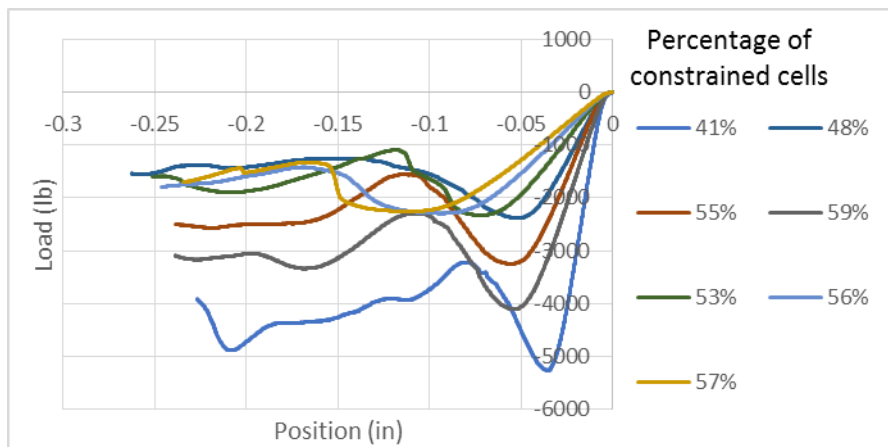


Figure B9. Graphs of load vs. position of equilateral triangle specimens that had more than 60% of constrained cells.

References

1. C. Neff, N. Hopkinson, N.B. Crane, "Selective Laser Sintering of Diamond Lattice Structures: Experimental Results and FEA Model Comparison," 2015 Solid Freeform Fabrication Symposium
2. M. Jamshidinia, L. Wang, W. Tong, and R. Kovacevic. "The bio-compatible dental implant designed by using non-stochastic porosity produced by Electron Beam Melting®(EBM)," *Journal of Materials Processing Technology* 214, no. 8 (2014): 1728-1739
3. S. Park, D.W. Rosen, C.E. Duty, "Comparing Mechanical and Geometrical Properties of Lattice Structure Fabricated using Electron Beam Melting", 2014 Solid Freeform Fabrication Symposium
4. D.M. Correa, T. Klatt, S. Cortes, M. Haberman, D. Kovar, C. Seepersad, "Negative stiffness honeycombs for recoverable shock isolation," *Rapid Prototyping Journal*, 2015, 21(2), pp.193-200
5. C. Yan, L. Hao, A. Hussein, P. Young, and D. Raymont. "Advanced lightweight 316L stainless steel cellular lattice structures fabricated via selective laser melting," *Materials & Design* 55 (2014): 533-541
6. S. Didam, B. Eidel, A. Ohrndorf, H.-J Christ. "Mechanical Analysis of Metallic SLM - Lattices on Small Scales: Finite Element Simulations versus Experiments," *PAMM* 15.1 (2015): 189-190
7. P. Zhang, J. Toman, Y. Yu, E. Biyikli, M. Kirca, M. Chmielus, and A.C. To. "Efficient design-optimization of variable-density hexagonal cellular structure by additive manufacturing: theory and validation," *Journal of Manufacturing Science and Engineering* 137, no. 2, 2015
8. M. Mazur, M. Leary, S. Sun, M. Vcelka, D. Shidid, M. Brandt. "Deformation and failure behaviour of Ti-6Al-4V lattice structures manufactured by selective laser melting (SLM)," *The International Journal of Advanced Manufacturing Technology* 84.5, 2016, 1391-1411
9. R. Gümruk, R.A.W. Mines, "Compressive behaviour of stainless steel micro-lattice structures," *International Journal of Mechanical Sciences* 68, 2013, 125-139
10. S. Ahmadi, G. Campoli, S. Amin Yavari, B. Sajadi, R. Wauthle, J. Schrooten, H. Weinans, A. Zadpoor, A., 2014, "Mechanical behavior of regular open-cell porous biomaterials made of diamond lattice unit cells," *Journal of the Mechanical Behavior of Biomedical Materials*, 34, 106-115.
11. S. Zhang, S. Dilip, L. Yang, H. Miyanji, B. Stucker, "Property Evaluation of Metal Cellular Strut Structures via Powder Bed Fusion AM," 2015 Solid Freeform Fabrication Symposium
12. D. Bhate, J. Van Soest, J. Reeher, D. Patel, D. Gibson, J. Gerbasi, and M. Finfrock, "A Validated Methodology for Predicting the Mechanical Behavior of ULTEM-9085 Honeycomb Structures Manufactured by Fused Deposition Modeling," *Proceedings of the 26th Annual International Solid Freeform Fabrication*, 2016, pp. 2095-2106
13. L. J. Gibson and M. F. Ashby, "*Cellular solids: Structure and properties*," 2nd ed. Cambridge: Cambridge University Press, 1997.
14. P. R. Onck, E. W. Andrews, L. J. Gibson. Size effects in ductile cellular solids. Part I: modeling. *International Journal of Mechanical Sciences*. 43, 2001, pp 681-699.

15. E. W. Andrews, G. Gioux, P. Onck, L. J. Gibson. Size effects in ductile cellular solids. Part II: experimental results. *International Journal of Mechanical Sciences*, 43, 2001, pp 701-713.
16. O. Kesler, L. J. Gibson. Size effects in metallic foam core sandwich beams. *Materials Science and Engineering A*. 326, 2002, pp 228-234.
17. J. F. Rakow, A. M. Waas, "Size effects and the shear response of aluminum foam," *Mechanics of Materials*, 37, 2005, pp 69-82
18. C. Tekoglu, P. R. Onck. Size effects in the mechanical behavior of cellular materials. *Journal of Materials Science*. 40, 2005, 5911-5917.
19. G. Dai, W. Zhang. Size effects of effective Young's modulus for periodic cellular materials. *Science in China Series G: Physics, Mechanics and Astronomy*, 52, 2009, pp. 1262-1270.
20. L. Yang, "A study about size effects of 3D periodic cellular structures," *Proceedings of the 26th Annual International Solid Freeform Fabrication*, 2016, pp. 2095-2106
21. Steve Lampman (editor), "*Characterization and Failure Analysis of Plastics*," 1st ed., ASM International, 2003
22. S. Malek and L. Gibson. Effective elastic properties of periodic hexagonal honeycombs. *Mechanics of Materials* 91pp. 226-240. 2015. . DOI: 10.1016/j.mechmat.2015.07.008
23. Stratasys Inc., "ABS-30 Production-Grade Thermoplastic for Fortus 3D Production Systems," Specification Sheet, accessed online May 2017